3 | Results for spherical nuclei

In this chapter, results for spherical nuclei are presented. These are mostly calculated for double magic nuclei, with the exception of ^{90}Zr.
Numerous spherical HF codes are available, they have the advantage of being one-dimensional, which allows the use of very fine meshes, with a step size that can go down to the physical scale of the problem, which is roughly 0.1 fm in this case, without any major computational limit. We can use these codes as a reference ideal value for the different quantities produced by our code. The choice for benchmarking in the present work has been the `hfbcs_qrpa` code [6].

3.1. Physical quantities

After finding a nucleus ground state, we are able to compute numerous physical properties of the system. We can use these values as a numerical reference when comparing our results with other codes.

3.1.1. Mean square radii

An important set of parameters characterizing the nuclear density is certainly the one of mean square radii.
The individual nuclear spieces' mean square radius is defined as

$$\langle r_q^2 \rangle = \frac{\int \rho_q(\boldsymbol{r}) r^2 d\boldsymbol{r}}{\int \rho_q(\boldsymbol{r}) d\boldsymbol{r}} \tag{3.1}$$

While the charge mean square radius formula is derived from the convolution of the neutron and proton particle densities with their respective internal charge distribution [1], resulting in equation 3.2.

$$\langle r_{ch}^2 \rangle = \langle r_p^2 \rangle + \langle r^2 \rangle_P + \frac{N}{Z} \langle r^2 \rangle_N + \frac{2}{Z} \left(\frac{\hbar}{mc} \right)^2 \sum_{\alpha q} \mu_q \langle \boldsymbol{\sigma} \cdot \boldsymbol{\ell} \rangle_{\alpha q} \tag{3.2}$$

where q runs over the nuclear species and α runs over all single particle states. $\boldsymbol{\sigma}$ is the vector operator of Pauli matrices, while $\boldsymbol{\ell}$ is the angular momentum operator $-i(\boldsymbol{r} \times \nabla)$. $\langle r^2 \rangle_P$ and $\langle r^2 \rangle_N$ refer to the square charge radii of the proton and the neutron, while μ_q to their respective magnetic dipole moment in units of nuclear magneton.
All square charge radii computed in this work use the set of parameters in table 3.1.

Parameter	Value	Units
$\langle r^2 \rangle_P$	0.64	fm^2
$\langle r^2 \rangle_N$	-0.11	fm^2
μ_p	2.792847	-
μ_n	-1.913043	-

Table 3.1: Parameters used to compute the charge mean square radius

3.1.2. Deformation parameters

When dealing with deformed nuclei, mean square radii are not sufficient to characterize the nuclear density. The main parameter used is the deformation parameter β, defined already in section (REF), it can be computed through the actual mean square radius with formula 3.3

$$\beta_2 = \frac{4\pi \langle Y_{20} \rangle}{3A \langle r^2 \rangle} \tag{3.3}$$

Where $\langle r^2 \rangle$ is the total mean square radius of the nucleus

$$\langle r^2 \rangle = \frac{\int (\rho_n + \rho_p) r^2 d\boldsymbol{r}}{\int (\rho_n + \rho_p) d\boldsymbol{r}} = \langle x^2 + y^2 + z^2 \rangle . \tag{3.4}$$

For spherical nuclei, $\beta_2 = 0$, while for deformed ones, thanks to the normalization with respect to the total radius and mass, the β_2 parameter can be used to compare different nuclei across the nuclide chart.

3.2. Parameters and mesh choice

All `hfbcs_qrpa` calculations are performed using a mesh size of 0.1 fm, no pairing interaction, and a radial mesh size that corresponds to the one chosen for our computation. The lattice of our code will depend on the extension of the nucleus, since the number of subdivisions that allows reasonable CPU times on a laptop caps around $60-70$. For ^{16}O, we are able to reach a 0.3 fm step size, while for the heaviest, the ^{90}Zr, we are only able to reach 0.42 fm. The reason behind this choice is that as the nucleus size increases, a bigger box

is needed to ensure that weakly bound states are able to decay to zero at the boundary. All the data reported in this chapter is computed with the SLy5 parametrization.

3.3. Results for ^{16}O

The first results we will take a look at are the ones for ^{16}O. It's the best candidate for gauging the solver's performance, as it is a light, double magic nucleus, meaning it has no pairing interaction and a spherical shape.
All calculations are performed on a box of size $[-9, 9]$ fm in all three directions and a step size of 0.3 fm, correponding to 60 subdivisions.

3.3.1. Results neglecting Coulomb interaction

As a case study, we will start by looking at results for increasing terms in the functional. Starting from the ones for C_0^ρ, C_1^ρ, C_0^τ, C_1^τ reported in table 3.2, neglecting the Coulomb interaction. Without further terms, the spin-orbit field $\boldsymbol{B}(\boldsymbol{r})$ is null, hence the $1p_{3/2}$ and $1p_{1/2}$ levels are degenerate.
Since $N = Z$, the single-particle equations will be exactly equal between the two species, assuming equal mass, therefore only neutron results are reported. Note that C_1 terms reduce to being null in this case, that is until we either break the $N = Z$ equality or introduce Coulomb terms. In table 3.3 the $C_0^{\boldsymbol{\nabla}\cdot\boldsymbol{J}}$ and $C_1^{\boldsymbol{\nabla}\cdot\boldsymbol{J}}$ terms are included just for the

Physical quantities

		GCG	hfbcs_qrpa	Δ	Δ%
E_{TOT}	[MeV]	-141.582	-141.582	-	-
$\langle r_n^2 \rangle^{1/2}$	[fm]	2.6504	2.6510	0.0006	2.26×10^{-2}
$\langle r_{ch}^2 \rangle^{1/2}$	[fm]	2.7486	2.7491	0.0005	1.82×10^{-2}

Neutron energy levels

		GCG	hfbcs_qrpa	Δ	Δ%
$1s_{1/2}$	[MeV]	-36.142	-36.139	0.003	8.30×10^{-3}
$1p_{3/2}$	[MeV]	-18.573	-18.572	0.001	5.38×10^{-3}
$1p_{1/2}$	[MeV]	-18.573	-18.572	0.001	5.38×10^{-3}

Table 3.2: ^{16}O including C_0^ρ, C_1^ρ, C_0^τ, C_1^τ terms, neglecting Coulomb interaction.

spin-orbit field $\boldsymbol{B}(\boldsymbol{r})$, but not for the mean field $U(\boldsymbol{r})$; from an interaction point of view, it's as if we were neglecting the spin-gradient coupling term [4].

Physical quantities

		GCG	hfbcs_qrpa	Δ	Δ%
E_{TOT}	[MeV]	-142.080	-142.080	-	-
$\langle r_n^2 \rangle^{1/2}$	[fm]	2.6516	2.6516	-	-
$\langle r_{ch}^2 \rangle^{1/2}$	[fm]	2.7497	2.7497	-	-

Neutron energy levels

		GCG	hfbcs_qrpa	Δ	Δ%
$1s_{1/2}$	[MeV]	-36.314	-36.312	0.002	5.5×10^{-3}
$1p_{3/2}$	[MeV]	-20.696	-20.696	-	-
$1p_{1/2}$	[MeV]	-14.335	-14.335	-	-

Table 3.3: ^{16}O including C_0^{ρ}, C_1^{ρ}, C_0^{τ}, C_1^{τ}, $C_0^{\boldsymbol{\nabla \cdot J}}$, $C_1^{\boldsymbol{\nabla \cdot J}}$ terms, neglecting Coulomb interaction and spin-gradient coupling.

Lastly, in table 3.4, the $C_0^{\boldsymbol{\nabla \cdot J}}$ and $C_1^{\boldsymbol{\nabla \cdot J}}$ terms are also included in the calculation of the mean-field.

Physical quantities

		GCG	hfbcs_qrpa	Δ	Δ%
E_{TOT}	[MeV]	-142.074	-142.074	-	-
$\langle r_n^2 \rangle^{1/2}$	[fm]	2.6515	2.6516	0.0001	3.77×10^{-3}
$\langle r_{ch}^2 \rangle^{1/2}$	[fm]	2.7497	2.7497	-	-

Neutron energy levels

		GCG	hfbcs_qrpa	Δ	Δ%
$1s_{1/2}$	[MeV]	-36.309	-36.308	0.001	2.75×10^{-3}
$1p_{3/2}$	[MeV]	-20.684	-20.685	0.001	4.83×10^{-3}
$1p_{1/2}$	[MeV]	-14.361	-14.361	-	-

Table 3.4: ^{16}O neglecting Coulomb interaction.

Results including Coulomb interaction

In table 3.5 results for the full Skyrme functional and the Coulomb interaction are presented.

Physical quantities

		GCG	hfbcs_qrpa	Δ	Δ%
E_{TOT}	[MeV]	-128.402	-128.400	0.002	1.56×10^{-3}
$\langle r_n^2 \rangle^{1/2}$	[fm]	2.6584	2.6585	0.0001	3.76×10^{-3}
$\langle r_p^2 \rangle^{1/2}$	[fm]	2.6835	2.6836	0.0001	3.73×10^{-3}
$\langle r_{ch}^2 \rangle^{1/2}$	[fm]	2.7805	2.7803	0.0002	7.19×10^{-3}

Neutron energy levels

		GCG	hfbcs_qrpa	Δ	Δ%
$1s_{1/2}$	[MeV]	-36.140	-36.137	0.003	8.30×10^{-3}
$1p_{3/2}$	[MeV]	-20.611	-20.611	-	-
$1p_{1/2}$	[MeV]	-14.427	-14.428	0.001	6.93×10^{-3}

Proton energy levels

		GCG	hfbcs_qrpa	Δ	Δ%
$1s_{1/2}$	[MeV]	-32.349	-32.345	0.004	1.24×10^{-2}
$1p_{3/2}$	[MeV]	-17.137	-17.137	-	-
$1p_{1/2}$	[MeV]	-11.081	-11.082	0.001	9.02×10^{-3}

Table 3.5: ^{16}O complete of the Skyrme functional and Coulomb interaction.

3.4. Results for heavier nuclei

In the following section, results for spherical nuclei heavier than ^{16}O are presented.

Physical quantities

		GCG	hfbcs_qrpa	Δ	Δ%
E_{TOT}	[MeV]	-415.955	-415.931	0.024	5.77×10^{-3}
$\langle r_n^2 \rangle^{1/2}$	[fm]	3.6106	3.6110	0.0004	1.11×10^{-2}
$\langle r_p^2 \rangle^{1/2}$	[fm]	3.4502	3.4507	0.0005	1.45×10^{-2}
$\langle r_{ch}^2 \rangle^{1/2}$	[fm]	3.5274	3.5060	0.0214	0.610

Neutron energy levels

		GCG	hfbcs_qrpa	Δ	Δ%
$1s_{1/2}$	[MeV]	-49.758	-49.752	0.006	1.21×10^{-2}
$1p_{3/2}$	[MeV]	-35.952	-35.949	0.003	8.34×10^{-3}
$1p_{1/2}$	[MeV]	-33.891	-33.891	-	-
$1d_{5/2}$	[MeV]	-22.170	-22.169	0.001	4.51×10^{-3}
$2s_{1/2}$	[MeV]	-17.720	-17.720	-	-
$1d_{3/2}$	[MeV]	-17.431	-17.434	0.003	1.72×10^{-2}
$1f_{7/2}$	[MeV]	-9.262	-9.261	0.001	1.08×10^{-2}

Proton energy levels

		GCG	hfbcs_qrpa	Δ	Δ%
$1s_{1/2}$	[MeV]	-45.936	-45.930	0.006	1.31×10^{-2}
$1p_{3/2}$	[MeV]	-34.314	-34.311	0.003	8.74×10^{-3}
$1p_{1/2}$	[MeV]	-30.482	-30.483	0.001	3.28×10^{-3}
$1d_{5/2}$	[MeV]	-22.455	-22.454	0.001	4.45×10^{-3}
$2s_{1/2}$	[MeV]	-16.753	-16.751	0.002	1.19×10^{-2}
$1d_{3/2}$	[MeV]	-15.337	-15.340	0.003	1.96×10^{-2}

Table 3.6: ^{48}Ca, box size [-12, 12] fm, step size 0.34 fm

Physical quantities

		GCG	hfbcs_qrpa	Δ	Δ%
E_{TOT}	[MeV]	-482.805	-482.700	0.105	2.18×10^{-2}
$\langle r_n^2 \rangle^{1/2}$	[fm]	3.6422	3.6433	0.0011	3.02×10^{-2}
$\langle r_p^2 \rangle^{1/2}$	[fm]	3.6968	3.6979	0.0011	2.97×10^{-2}
$\langle r_{ch}^2 \rangle^{1/2}$	[fm]	3.7722	3.7682	0.0040	0.106

Neutron energy levels

		GCG	hfbcs_qrpa	Δ	Δ%
$1s_{1/2}$	[MeV]	-54.277	-54.260	0.017	3.13×10^{-2}
$1p_{3/2}$	[MeV]	-41.571	-41.562	0.009	2.16×10^{-2}
$1p_{1/2}$	[MeV]	-39.613	-39.611	0.002	5.05×10^{-3}
$1d_{5/2}$	[MeV]	-28.536	-28.530	0.006	2.10×10^{-2}
$2s_{1/2}$	[MeV]	-23.539	-23.545	0.006	2.55×10^{-2}
$1d_{3/2}$	[MeV]	-23.367	-23.361	0.006	2.57×10^{-2}
$1f_{7/2}$	[MeV]	-16.019	-16.018	0.001	6.24×10^{-3}

Proton energy levels

		GCG	hfbcs_qrpa	Δ	Δ%
$1s_{1/2}$	[MeV]	-43.754	-43.740	0.014	3.20×10^{-2}
$1p_{3/2}$	[MeV]	-31.561	-31.555	0.006	1.90×10^{-2}
$1p_{1/2}$	[MeV]	-29.545	-29.545	-	-
$1d_{5/2}$	[MeV]	-19.017	-19.016	0.001	5.26×10^{-3}
$2s_{1/2}$	[MeV]	-14.004	-14.012	0.008	5.71×10^{-2}
$1d_{3/2}$	[MeV]	-13.891	-13.887	0.004	2.88×10^{-2}
$1f_{7/2}$	[MeV]	-6.934	-6.935	0.001	1.44×10^{-2}

Table 3.7: ^{56}Ni, box size [-13, 13] fm, step size 0.37 fm

Physical quantities

		GCG	hfbcs_qrpa	Δ	Δ%
E_{TOT}	[MeV]	-783.587	-783.325	0.262	3.34×10^{-2}
$\langle r_n^2 \rangle^{1/2}$	[fm]	4.2854	4.2872	0.0018	4.20×10^{-2}
$\langle r_p^2 \rangle^{1/2}$	[fm]	4.2196	4.2212	0.0016	3.79×10^{-2}
$\langle r_{ch}^2 \rangle^{1/2}$	[fm]	4.2767	4.2704	0.0063	0.148

Neutron energy levels

		GCG	hfbcs_qrpa	Δ	Δ%
$1s_{1/2}$	[MeV]	-55.636	-55.615	0.021	3.78×10^{-2}
$1p_{3/2}$	[MeV]	-45.324	-45.309	0.015	3.31×10^{-2}
$1p_{1/2}$	[MeV]	-44.172	-44.160	0.012	2.72×10^{-2}
$1d_{5/2}$	[MeV]	-34.148	-34.137	0.011	3.22×10^{-2}
$2s_{1/2}$	[MeV]	-31.393	-31.391	0.002	6.37×10^{-3}
$1d_{3/2}$	[MeV]	-29.802	-29.797	0.005	1.68×10^{-2}
$1f_{7/2}$	[MeV]	-22.755	-22.748	0.007	3.08×10^{-2}
$2p_{3/2}$	[MeV]	-17.837	-17.840	0.003	1.68×10^{-2}
$1f_{5/2}$	[MeV]	-17.568	-17.563	0.005	2.85×10^{-2}
$2p_{1/2}$	[MeV]	-15.729	-15.723	0.006	3.82×10^{-2}
$1g_{9/2}$	[MeV]	-11.586	-11.580	0.006	5.18×10^{-2}

Proton energy levels

		GCG	hfbcs_qrpa	Δ	Δ%
$1s_{1/2}$	[MeV]	-44.973	-44.956	0.017	3.78×10^{-2}
$1p_{3/2}$	[MeV]	-36.347	-36.336	0.011	3.03×10^{-2}
$1p_{1/2}$	[MeV]	-34.121	-34.115	0.006	1.76×10^{-2}
$1d_{5/2}$	[MeV]	-26.766	-26.759	0.007	2.62×10^{-2}
$2s_{1/2}$	[MeV]	-22.175	-22.178	0.003	1.35×10^{-2}
$1d_{3/2}$	[MeV]	-21.216	-21.214	0.002	9.43×10^{-3}
$1f_{7/2}$	[MeV]	-16.722	-16.718	0.004	2.39×10^{-2}
$2p_{3/2}$	[MeV]	-10.239	-10.236	0.003	2.93×10^{-2}
$1f_{5/2}$	[MeV]	-9.613	-9.618	0.005	5.20×10^{-2}
$2p_{1/2}$	[MeV]	-8.108	-8.104	0.004	4.94×10^{-2}

Table 3.8: ^{90}Zr, box size [-15, 15] fm, step size 0.43 fm

4 | Results for deformed nuclei

Having established that the code works well for spherical nuclei, we can start treading in deformation territory.

4.1. ^{24}Mg

In the following section, results for ^{24}Mg are presented, it's a natural choice to study how well deformations are represented by our framework, since it's light, very deformed and shows no pairing interaction in its ground state.

4.1.1. HFBTHO code and calculation details

HFBTHO

To benchmark the code in the case of nuclear deformation, the HFBTHO code was used [21], it's a HFB code which minimizes the energy functional on a (Transformed) Harmonic Oscillator basis. Since ^{24}Mg is a light nucleus, it still works well in this case.
All calculations are carried out using a number of shells of 12 and a null pairing interaction. Default paramters for the quadrupole constraints were used.

Code parameters and axial constraint

As for our code, calculations are performed on a box $[-10, 10]$ fm. In the case of the ground state calculation, a step size of 0.33 fm is used, with a starting guess of a deformed Woods-Saxon with $\beta_2 = 0.4$.
The calculation in the case of the deformation curve is carried out imposing the following constraints

$$\langle \mathrm{Re}\, \mathcal{Q}_{22} \rangle = 0 \tag{4.1}$$

$$\langle \mathrm{Im}\, \mathcal{Q}_{22} \rangle = 0 \tag{4.2}$$

$$\langle \mathcal{Q}_{20} \rangle = q_{20}. \tag{4.3}$$

These constraints altogether impose an axial deformation on the system. This is done because on a full mesh like in our case, the nucleus may deform on a different axis from the chosen one (z), resulting in spurious contributions to the real deformation curve; moreover, the axial symmetry of `HFBTHO` doesn't allow broken axial symmetry configurations.
Regarding the stiffness c and damping parameter μ of ALM 2.3.1, $c = 0.001$ and $\mu = 0.1$ were used. As for convergence criteria, a tolerance of 0.001 on the value of $\beta_2 - \beta_{2,\text{target}}$ was used.

Ground state

Table 4.1 reports data for the ground state of ^{24}Mg, compare with `HFBTHO` results, while figure 4.1 shows the total particle density. Charge radii for the two codes are displayed but not compared, due to different formulas used for their computation.

		GCG	`HFBTHO`	Δ	Δ%
E_{TOT}	[MeV]	-195.854	-197.030	1.176	0.597
$\langle r_n^2 \rangle^{1/2}$	[fm]	3.0124	2.9996	0.0128	0.427
$\langle r_p^2 \rangle^{1/2}$	[fm]	3.0475	3.0326	0.0149	0.491
$\langle r_{ch}^2 \rangle^{1/2}$	[fm]	3.5390	3.4614	-	-
$\langle z^2 \rangle^{1/2}$	[fm]	2.1454	-	-	-
$\langle x^2 \rangle^{1/2}$	[fm]	1.5112	-	-	-
$\langle y^2 \rangle^{1/2}$	[fm]	1.5147	-	-	-
β_2	[-]	0.399	0.390	0.009	2.3

Table 4.1: Results for ^{24}Mg ground state, no pairing interaction, box $[-10, 10]$ fm, step size 0.33 fm, SKM* parametrization.

Deformation curve

In figure 4.2, the deformation curve is shown for ^{24}Mg, without pairing. To counteract the sharp rise in CPU time, due to the high number of points in the curve, a coarser grid is used, hence the different minimum energy and β_2 values than the ones reported in table 4.1.

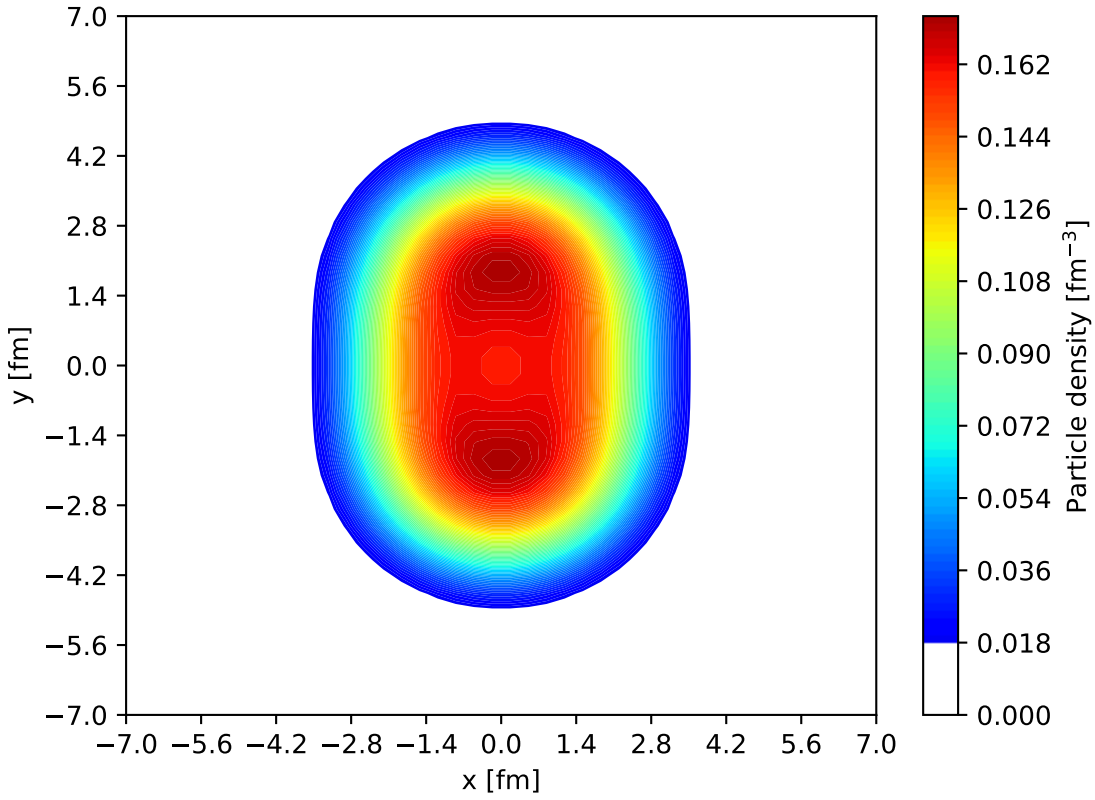

Figure 4.1: Magnesium ground state density, calculation done on a box $[-10, 10]$ fm, step size 0.33 fm, SKM* parametrization

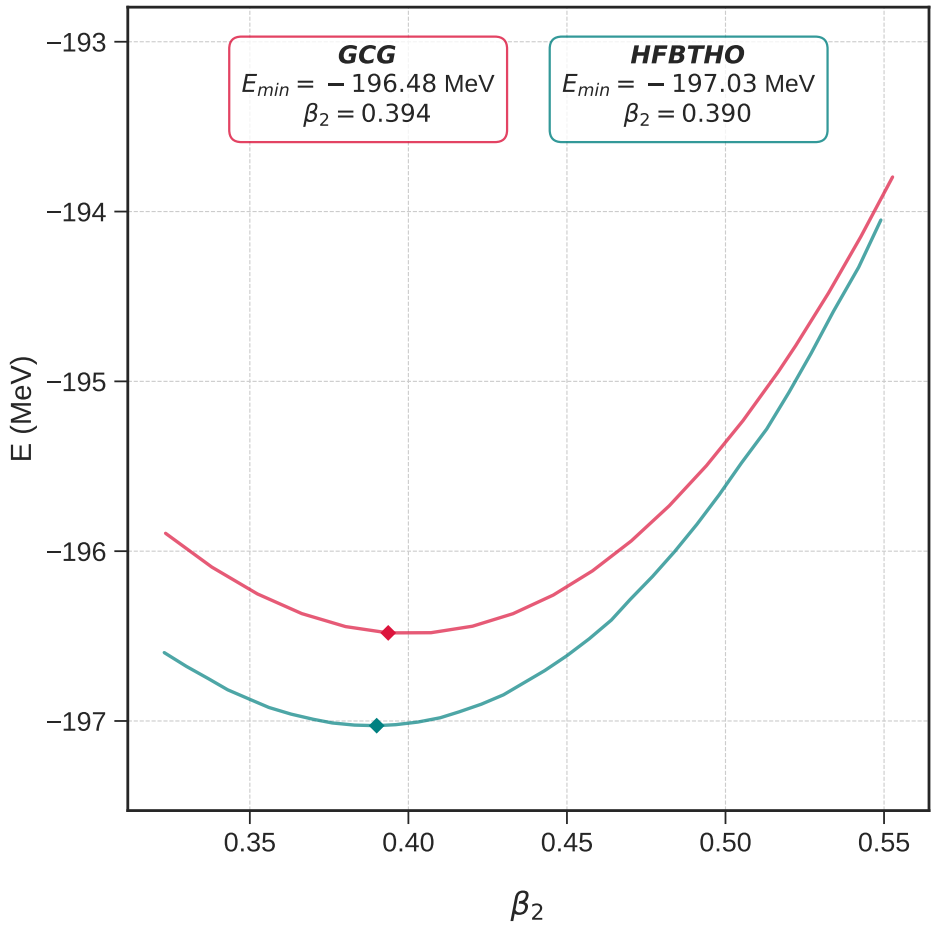

Figure 4.2: Magnesium deformation curve, no pairing interaction, calculation done on a box $[-10, 10]$ fm, step size 0.66 fm, SKM* parametrization.